Project No. 12-3306

Nonlinear Ultrasonic Techniques to Monitor Radiation Damage in RPV and Internal Components

Light Water Reactor Sustainability

Laurence Jacobs
Georgia Institute of Technology

In collaboration with:
Northwestern University
Electric Power Research Institute
Pacific Northwest National Laboratory

Richard Reister, Federal POC
Jeremy Busby, Technical POC

NEUP Nuclear Energy University Programs
U.S. Department of Energy

Final Report

Project Title: Nonlinear Ultrasonic Techniques to Monitor Radiation Damage in RPV and Internal Components

Covering Period: August 1, 2012-September 30, 2015

Date of Report: November 2, 2015

Recipient: Georgia Tech Research Corporation

Principal Investigator: Laurence Jacobs, 404-894-2344. laurence.jacobs@coe.gatech.edu
Co-PIs: Jin-Yeon Kim, jykim@gatech.edu, Jianmin Qu, j-qu@northwestern.edu, Pradeep Ramuhalli, pradeep.ramuhalli@pnnl.gov, Joe Wall, jwall@epri.com

Project Objective: The objective of this research is to demonstrate that nonlinear ultrasonics (NLU) can be used to directly and quantitatively measure the remaining life in radiation damaged reactor pressure vessel (RPV) and internal components. Specific damage types to be monitored are irradiation embrittlement and irradiation assisted stress corrosion cracking (IASCC). Our vision is to develop a technique that allows operators to assess damage by making a limited number of NLU measurements in strategically selected critical reactor components during regularly scheduled outages. This measured data can then be used to determine the current condition of these key components, from which remaining useful life can be predicted. Methods to unambiguously characterize radiation related damage in reactor internals and RPVs remain elusive. NLU technology has demonstrated great potential to be used as a *material sensor* – a sensor that can continuously monitor a material's damage state. The physical effect being monitored by NLU is the generation of higher harmonic frequencies in an initially monochromatic ultrasonic wave. The degree of nonlinearity is quantified with the acoustic nonlinearity parameter, β, which is an absolute, measurable material constant. Recent research has demonstrated that *nonlinear* ultrasound can be used to characterize material state and changes in microscale characteristics such as internal stress states, precipitate formation and dislocation densities. Radiation damage reduces the fracture toughness of RPV steels and internals, and can leave them susceptible to IASCC, which may in turn limit the lifetimes of some operating reactors. The ability to characterize radiation damage in the RPV and internals will enable nuclear operators to set operation time thresholds for vessels and prescribe and schedule replacement activities for core internals. Such a capability will allow a more clear definition of reactor safety margins. The research consists of three tasks: (1) materials sensing and monitoring; (2) physics-based materials and damage evolution modeling; and (3) remaining life estimation by integrating sensing, modeling and uncertainty.

1. Final Report

1.1 Summary

The overall objectives of this research were to: 1. demonstrate that nonlinear ultrasonics (NLU) is sensitive to irradiation damage; 2. develop a physics-based materials model to track radiation damage; 3. integrate sensing, modeling and uncertainty for remaining life estimation; and 4. use NLU to directly and quantitatively measure the remaining life in radiation damaged reactor pressure vessel (RPV) steels and internal components. Work was performed on each of these objectives as described below. In summary *objective one* was fully met, where NLU was demonstrated to be sensitive to irradiation damage. Work on the modeling and measurements partially met the objectives of *objective two*, mainly through the use of surrogate specimens to model the precipitate formation and interaction with dislocations seen in irradiation damage; these results are also described below. *Objective three* was partially met through the development of a procedure that used noncontact air-coupled transducers plus a procedure to make absolute measurements in complex components. Finally, *objective three* was partially met with an emphasis on uncertainty in the measured nonlinearity and an attempt to relate these values to overall material performance, including a multi-physics approach with magnetic Barkhausen noise.

Overall, the research resulted in eight published papers, two currently under review and three in preparation. Radiation damage in RPV steels causes microstructural changes that leave the material in an embrittled state. Nonlinear ultrasound is an NDE technique quantified by the measurable acoustic nonlinearity parameter, which is sensitive to microstructural changes in metallic materials such as dislocations, precipitates and their combinations. This research first demonstrated the sensitivity of the acoustic nonlinearity parameter to increasing neutron fluence in representative RPV steels. It then considered nonlinear ultrasonic experiments conducted on similar RPV steel samples that had a combination of irradiation, annealing, re-irradiation, and/or re-annealing to a total neutron fluence of 0.5-5x10^{19} n/cm^2 (E > 1 MeV) at an irradiation temperature of 290°C. The acoustic nonlinearity parameter generally increased with increasing neutron fluence, and consistently decreased from the irradiated to the annealed state over different levels of neutron fluence. Results of the measured acoustic nonlinearity parameter are compared with those from previous measurements on other RPV steel samples. This comprehensive set of results illustrates the dependence of the measured acoustic nonlinearity parameter on neutron fluence, material composition, irradiation temperature and annealing (Matlack et al, *JNM* 2014, Matlack et al ASTM STP 1576, 2014).

Since the main contributor of irradiation damage is copper-rich precipitates, 17-4PH stainless steel is thermally aged to study the effects of copper precipitates on the acoustic nonlinearity parameter. Nonlinear ultrasonic measurements using Rayleigh waves are performed on isothermally aged 17-4PH. Results showed a decrease in the acoustic nonlinearity parameter with increasing aging time, consistent with evidence of copper precipitation from hardness, thermo-electric power, transmission electron microscopy, and atom probe tomography measurements (Matlack et al, *NDT&E Intl* 2015).

Additional work measures the ultrasonic nonlinearity parameter as an indicator of thermal damage in 9%Cr ferritic martensitic steel specimens. The specimens are isothermally aged for different holding periods. As thermal aging progresses, the existing dislocations are

annihilated in the beginning and precipitates are formed; these microstructural evolutions lead to large changes in the measured nonlinearity parameter, β. A possible scenario for the microstructural evolution during thermal aging is proposed based on the results from the nonlinear ultrasonic measurements, scanning electron microscopy (SEM), and Rockwell HRC hardness. These results indicate a clear trend that the measured nonlinearity parameter is sensitive to variations in dislocation and precipitate density (Marino et al, *NDT&E Intl*, 2015).

For the integration of sensing and material behavior, a research effort quantifies the effects of diffraction, attenuation, and the nonlinearity of generating sources on measurements of nonlinear ultrasonic Rayleigh wave propagation. A revised theoretical framework for correcting measurements made with air-coupled and contact piezoelectric receivers for the aforementioned effects is provided based on analytical models and experimental considerations. A method for extracting the nonlinearity parameter β_{11} is proposed based on a nonlinear least squares curve-fitting algorithm that is tailored for Rayleigh wave measurements. Quantitative experiments are conducted to confirm the predictions for the nonlinearity of the piezoelectric source and to demonstrate the effectiveness of the curve-fitting procedure. These experiments are conducted on aluminum 2024 and 7075 specimens and a $\beta_{11}^{7075}/\beta_{11}^{2024}$ measure of 1.363 agrees well with previous literature and earlier work. The proposed work is also applied to a set of 2205 duplex stainless steel specimens that underwent various degrees of heat-treatment over 24 hours, and the results improve upon conclusions drawn from previous analysis (Torello et al, *Ultrasonic*s, 2015).

The implementation of the nonlinear ultrasonic technique in a hot cell environment was performed as a part of the US-Korea INERI program between Georgia Tech and KAERI. The objective of this research is to make attempts to bring promising NDE techniques developed for radiation damage characterization to more realistic situations. As a first step towards the ultimate field application in nuclear power plants, an in-situ measurement on a set of surveillance specimens in a hot-cell environment is considered. The NDE methods that are implemented in the hot cell at KAERI include the nonlinear ultrasonic technique of Georgia Tech and the magnetic Barkhausen noise/hysteresis loop measurement technique of KAERI.

The procedure to measure the second harmonic generation has typically been restricted to relatively simple setups such as through transmission of longitudinal waves or Rayleigh surface waves on one side of a component. Since these types of setups are not always applicable for in-service components, this research investigates the second harmonic wave generation in longitudinal and shear waves reflected from a stress-free surface.
This particular measurement setup potentially provides information about the local damage state in an in-service component with only single-sided access. Therefore, this measurement setup is evaluated analytically, numerically and experimentally with an aluminum specimen as an example. The setup being considered proposes two possible measurement positions, where the second harmonic and the fundamental wave amplitude can be measured to determine the nonlinearity parameter of the specimen. This proposed “reflection mode” setup is first analyzed analytically, and then is implemented in a commercial finite element code, using increasing fundamental wave amplitudes to calculate the different values of the nonlinearity parameters. The results of the simulations verify the analytical results, when taking into account assumptions and approximations of the analytical solution procedure.

Furthermore, these numerical finite element results provide further insights into the intricacies of the setup, including the need to avoid interaction with the diffracted waves. On the basis of these numerical results, a recommendation for the measurement position and angle is given. Finally, the nonlinearity parameters of two similar specimens with different levels of nonlinearity are experimentally measured with the proposed measurement setup, and the results (Romer et al, *JNDE*, 2015).

Finally from a modeling perspective, the research developed a model that considers the interaction of dislocations and precipitates to determine their influence on the measured acoustic nonlinearity parameter, β. Additional research derived the exact expressions for the isothermal third order elastic constants (TOE) in crystalline solids in terms of the kinetic and potential energies of the system. These expressions reveal that the TOE constants consist of a Born component and a relaxation component. The Born component is simply the third derivative of the system's potential energy with respect to the deformation, while the relaxation component is related to the non-uniform rearrangements of the atoms when the system is subjected to a macroscopic deformation. Based on the general expressions derived, a direct (fluctuation) method of computing the isothermal TOE constants is developed and numerical examples using this fluctuation method are given (Chen and Qu, *J App Phys*, 2015).

Refereed Journal Papers from the Research:

1. ***Marino*, D.,*** Kim, Jin-Yeon, Ruiz, Joo, Young-Sang, Qu, Jianmin, and Jacobs, L.J., "Using nonlinear ultrasound to track thermal aging damage in modified 9% Cr ferritic martensitic steel," *NDT&E International,* submitted, 2015.
2. ***Romer*, A.,*** Kim, Jin-Yeon, Qu, Jianmin and Jacobs, L.J., "The second harmonic generation in reflection mode – an analytical, numerical and experimental study," *Journal of Nondestructive Evaluation,* submitted, 2015.
3. ***Matlack*, K.H.., Bradley*, H.A., Thiele*, S,*** Kim, Jin-Yeon, Wall, J.J., Jung, Hee Joon, Qu, Jianmin, and Jacobs, L.J., "Nonlinear ultrasonic characterization of precipitation in 17-4PH stainless steel," *NDT&E International.,* Vol. 71, pp. 8-15, 2015.
4. Chen, Z. and Qu, Jianmin, "A fluctuation method to calculate the third order elastic constants in crystalline solids," *Journal of Applied Physics,* Vol. 117, 204902, 2015
5. ***Torello*, D., Thiele*, S., Matlack*, K.H.,*** Kim, Jin-Yeon, Qu, Jianmin, and Jacobs, L.J., "Diffraction, attenuation, and source corrections for nonlinear Rayleigh wave ultrasonic measurements," *Ultrasonics*, Vol. 56, pp. 417-426, 2015.
6. ***Matlack*, K.H.,*** Kim, Jin-Yeon, Jacobs, L.J., and Qu, Jianmin, "Review of second harmonic generation measurement techniques for material state determination in metals," *Journal of Nondestructive Evaluation,* DOI 10.1007/s 10921-014-0273-5, 2015.
7. ***Thiele*, S.,*** Kim, Jin-Yeon, Qu, Jianmin, and Jacobs, L.J, "Air-Coupled Detection of Nonlinear Rayleigh Surface Waves to Assess Material Nonlinearity," *Ultrasonics*, Vol. 54, pp. 1470-1475, 2014.
8. ***Matlack*, K.H.,*** Kim, Jin-Yeon, Wall, J.J, Qu, Jianmin, and Jacobs, L.J., "Nonlinear ultrasonic characterization of radiation damage using Charpy impact specimen," *JASTM STP 1576,* pp. 1-17, 2014
9. ***Matlack*, K.H.,*** Kim, Jin-Yeon, Wall, J.J, Qu, Jianmin, Jacobs, L.J, and Sokolov, M., "Sensitivity of ultrasonic nonlinearity to irradiated, annealed, and re-irradiated microstructure changes in RPV steels," *Journal of Nuclear Materials*, Vol. 448 pp. 26-32, 2014.

10. ***Scott*, K., Roach*, D.,*** Kim, Jin-Yeon, Wall, J.J., and Jacobs, L.J., "Development of nonlinear ultrasonic techniques to assess microstructural damage in 1% and 0.1% Fe-Cu Steel," *NDT&E International.*in preparation, 2015.
11. ***Torello*, D.,*** Kim, Jin-Yeon, Qu, Jianmin, and Jacobs, L.J., "Absolute measurements of the acoustic nonlinear parameter with non-contact, air-coupled detection," *Ultrasonics*, in preparation, 2015.
12. ***Uhrig*, M.,*** Kim, Jin-Yeon, and Jacobs, L.J., "3-D Simulation of nonlinear Rayleigh wave fields evaluation diffraction and attenuation effects in non-contact measurements," *Journal of Nondestructive Evaluation,* in preparation, 2015.

****Denotes co-author who is a current and/or former undergraduate or graduate research student funded by the project.***

2. Nonlinear Ultrasound to Characterize Damage in Irradiated Specimens

Consider the results presented in publication by Matlack et al in *JNM* [1] that examined the sensitivity of NLU to irradiated, annealed, and re-irradiated microstructure changes in RPV steels. Results for the measured nonlinearity parameter, β as a function of increasing fluence and the influence of post-irradiation annealing and re-irradiation of JRQ material irradiated at 290°C are given in Figure 1. Each data point represents an average over three separate measurements on the same sample at the same location, and error bars indicate one standard deviation from the mean. Separate data points for the same sample condition represent measurements on separate Charpy halves of the same sample condition, or measurements at different locations along the length of the Charpy half. The results in Figure 1 show little variation among locations and between different sample halves when compared to the changes due to irradiation and annealing; these spatial and sample variations in the same Charpy sample are shown to be insignificant. The measured β increased from the unirradiated state to the maximum neutron fluence, with a maximum increase of 18% at $5x10^{19}$ n/cm^2 (E > 1MeV). Results show a decrease in measured β from the irradiated condition (I or IAR) to the annealed condition (IA or IARA) – a 23.2% decrease due to annealing in the I,5 and IA,5 samples, and a 25.7% decrease due to annealing in the IAR,1.7 and IARA,1.7 samples. A summary of these changes in β due to neutron fluence and then due to annealing is given in Table 1. Note that the intermediate anneal in samples IAR,0.5 and IAR,1.7 effectively recovered most of the irradiation-induced embrittlement during the first irradiation to half the target fluence, so a more representative value for the neutron fluence of these samples in terms of β might be half the fluence listed in Table 1.

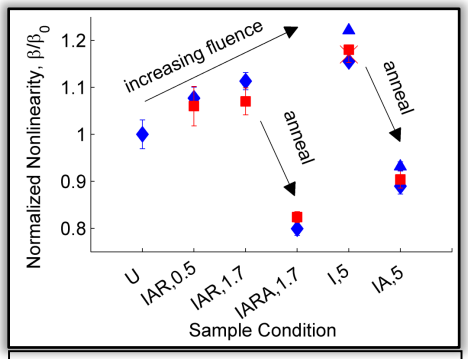

Fig.1: Experimental results of nonlinearity parameter dependence on increasing neutron fluence and annealing

Table 1: Change in β due to annealing and increased neutron fluence of JRQ (T_{ir} = 290°C).

Total Neutron fluence	$\Delta\beta$ from annealing	$\Delta\beta$ from irradiation
$0.5x10^{19}$ n/cm^2	--	+7%
$1.7x10^{19}$ n/cm^2	-25.7%	+9%
$5x10^{19}$ n/cm^2	-23.2%	+18%

Previous results for measured β for JRQ and JFL material at T_{ir} = 255°C as a function of increasing neutron fluence are shown together with the current results of measured β for irradiated JRQ at T_{ir} = 290°C in Figure 2. Results for JRQ at T_{ir} = 290°C in Figure 5 have been averaged over all measurements on different Charpy halves and different locations. Note that light water reactor pressure vessels typically operate at 290°C±30°, so the irradiation temperatures of the two data sets considered in this study approximate vessel operational conditions. These results are presented in terms of a normalized β to the unirradiated state in each sample set, i.e. $\beta_i/\beta_0 = \left(A_2/A_1^2\right)_i / \left(A_2/A_1^2\right)_0$. In this way, the dependence of β on the input fundamental radial frequency, ω, is eliminated, such that different excitation frequencies used in the measurements (f = 2.25 MHz for T_{ir} = 255°C and f = 3.3 MHz for T_{ir} = 290°C, where $\omega = 2\pi f$) do not influence the relative comparison of the measured β. Note that differences in fundamental frequency were due to limitations in equipment during earlier experiments – higher frequencies are more ideal for the shorter wave propagation distances encountered in these experiments, since the shorter wavelength allows more cycles and thus higher amplitude of A_2, given the same sample thickness.

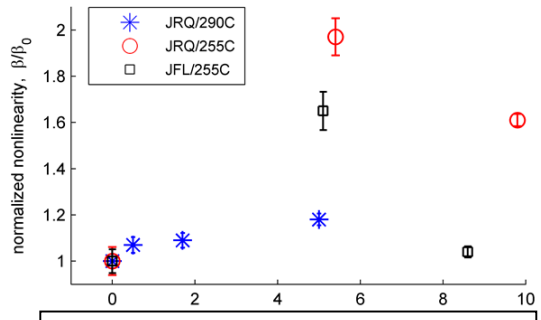

Figure 2: Influence of increasing neutron fluence (E > 1MeV) on β, for JRQ and JFL at T_{ir}=255°C and 290°C. Each dataset is normalized to the measured β in the unirradiated state, β_0. JRQ samples irradiated at 290°C to 0.5 x10^{19} and 1.7x10^{19} n/cm^2 received an intermediate anneal at 50% target fluence.

The trend of β as a function of neutron fluence for the irradiated JRQ at T_{ir}=290°C is similar to the trend shown in the previous work [2] and as seen in Figure 5 – an increase in β up to a medium fluence of roughly 5x10^{19} n/cm^2. However, the increase in β is much more pronounced in the samples with T_{ir} = 255°C, even in the low-copper alloy of JFL. At a neutron fluence of 5x10^{19} n/cm^2, it is shown that at T_{ir} = 255°C, β increased by almost 100% in JRQ and 65% in JFL, while at T_{ir} = 290°C, β increased by only 18% in JRQ, all from the respective unirradiated conditions of each sample set. These results show that the acoustic nonlinearity parameter strongly depends on the irradiation temperature as well as the level of neutron fluence.

3. Theoretical Modeling to Track Radiation Damage

Consider a sinusoidal longitudinal wave propagating at frequency ω through a weakly nonlinear elastic material. A second harmonic wave at frequency 2ω is generated through the interaction of the propagating wave with the nonlinear medium. The acoustic nonlinearity parameter, β, that quantifies this second harmonic wave has been shown to have the following relation [3]:

$$\beta = \frac{8A_2}{A_1^2 \kappa^2 x} \qquad (1)$$

where A_2 is the amplitude of the second harmonic wave generated, A_1 is the amplitude of the propagated first harmonic wave, κ is the wave number, and x is the wave propagation distance. It has previously been shown both theoretically and experimentally how different microstructural features that are relevant to radiation damage in RPV materials give rise to changes in β. The change in β due to a density of dislocations, Λ, that are pinned between two points to create a dislocation segment length of L_0, with some internal stress, σ_0, has been shown to be [3]:

$$\Delta\beta \propto \Lambda L_0^4 \sigma_0 . \quad (2)$$

This initial internal stress σ_0 is expected to be small, and note that the pinning points that create the dislocation segment length are features such as grain boundaries, other dislocations, and/or point defects.

Now assume that there is some distribution of precipitates embedded in the microstructure, which act as discrete pinning points for dislocations. We assume some number density of precipitates, N, with average radius r_p. For this case, the change in β has been shown to be [4-9]

$$\Delta\beta \propto \frac{\Lambda r_p^3}{N^{1/3}} . \quad (3)$$

Here, the stress in the material is due to a misfit strain of the precipitate embedded in the matrix, which is expected to be much larger than the initial stress σ_0. The full expression for the radial stress due to a spherical precipitate embedded in the microstructure can be found elsewhere [10, 11]. The relationship between segment length and number density of precipitates is assumed to be $L \approx 1/N^{1/3}$ as in previous work [9].

However, there should be some critical number density of precipitates, N_{cr}, only above which this precipitate-pinned dislocation contribution to β applies. The critical density corresponds to the density when all dislocations are pinned at least once in their lengths and therefore it is a constant multiple of the initial dislocation density. Above this critical density, additional precipitates will only shorten the lengths of the already-pinned dislocation segments. Therefore, the evolution of β is likely to follow some combination of the general dislocation pinning model (Equation (2)) and the precipitate-pinned dislocation model (Equation (3)), which can be expressed as:

$$\Delta\beta \propto (1-\alpha)\Lambda L_0^4 \sigma_0 + \alpha\Lambda \frac{r_p^3}{N^{1/3}} \quad (4)$$

where α represents the probability of forming the 3-precipitate cluster to bend an existing dislocation segment. This probability is close to zero at very low precipitate density, and is assumed to increase rapidly to 1 at N_{cr}. It is expected that α increases exponentially to 1 because the probability of an additional precipitate to interact with a dislocation depends on the precipitate concentration at the moment when the additional precipitate is added. Further, once the precipitate number density reaches N_{cr}, the chance for any additional nucleated precipitate to interact with a dislocation is nearly 100%. In this way, it is assumed the probability follows Boltzmann statistics, which represents the chance of a group of precipitates to form a specific configuration near a dislocation line, such that $\alpha = \exp(-B/N)$, where B is a positive number representing the precipitate configurational entropy and N is the current precipitate density.

The parameter α is also equivalent to the volume fraction of precipitate-pinned dislocation segments, such that the term $(1-\alpha)$ represents the volume fraction of dislocations pinned by

other features (e.g. grain boundaries, other dislocations, impurities, point defects, vacancies, or voids). Note that both the model of generally pinned dislocations (Equation (2)) and the model of precipitate-pinned dislocations (Equation (3)) cannot apply at the same time to the same dislocation segment – if a dislocation segment is pinned by two precipitates, that same segment cannot also be pinned by other features. It is expected that the first term in Equation (4) would dominate the behavior of β in the initial stages of radiation damage when precipitates are beginning to form. Then, as the number density of precipitates increases close to the N_{cr}, the second term in Equation (4) would dominate the trend of β.

4. Integrate Sensing, Modeling and Uncertainty for Remaining Life Estimation

In low-alloy steels under typical RPV conditions, neutron irradiation causes radiation-enhanced diffusion, which results in microstructural features such as copper-rich precipitates, solute clusters, matrix defects in the form of solute-vacancy complexes, and potentially dislocations and interstitial loops [12-14]. Considering the model described in Equation (4) for the change in β due to pinned dislocations, and assuming the precipitate-pinned contribution is stronger due to the higher stress induced by the precipitate misfit, β should *generally* increase by $\exp(-B/N)/N^{1/3}$ below N_{cr}, and decrease by $N^{1/3}$ above N_{cr}. The plot in Figure 3 illustrates this trend, and note that for simplicity we assume $B = 1$ such that the plot shows the function $\Delta\beta = \exp(-1/N)/N^{1/3}$. Since the change in $\Delta\beta$ over neutron fluence for $T_{ir} = 255°C$ changes sign at the medium fluence of roughly $5x10^{19}$ n/cm^2, we can infer that N_{cr} occurs roughly around this fluence level. Comparison of this model with experimental results suggest that in the JRQ samples irradiated at 290°C, the number density of precipitates is below N_{cr}, which explains the increasing measured β with increasing neutron fluence, and likely increasing number density of precipitates. This model qualitatively agrees with the experimental results, but suggests there are other microstructural features that contribute to the total $\Delta\beta$.

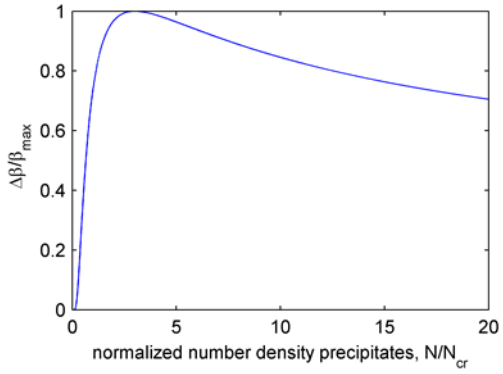

Figure 3: Predicted trend of $\Delta\beta$ (normalized by β_{max}) as a function of number density of precipitates, normalized by N_{cr}, assuming trend is dominated by precipitate-pinned dislocations (i.e. second term in Equation (4)).

Previously, small angle neutron scattering (SANS) experiments were conducted on the same JRQ and JFL samples with $T_{ir} = 255°C$ reported on here and previously [2], to quantify these microstructural features. The authors reported an increase in volume fraction of precipitates with constant average radius of about 1nm with increasing neutron fluence [15]. Specifically, the volume fraction increased from 0.005-0.09 vol. % for neutron fluence of 0.7-8.7x10^{19} n/cm^2 in JFL, and 0.21-0.5 vol. % for neutron fluence of 0.7-9.8x10^{19} n/cm^2 for JRQ. Considering the precipitate-pinned dislocation theory, this would imply that $\Delta\beta$ should be lower in JRQ compared to JFL, since JRQ has a higher volume fraction of copper rich precipitates. However, experimental evidence in Figure 2 shows the opposite – $\Delta\beta$ is larger for JRQ. Differences between the two materials such as dislocation density, grain structure (which would influence general dislocation pinning effects by grain boundaries), point defects and other defects, and

different N_{cr} could all contribute to this discrepancy. This again suggests that there are other microstructural features that contribute to the total $\Delta\beta$, and more microstructural characterizations are needed to explain this.

Microstructural changes over increasing neutron fluence are dependent on many other factors such as neutron flux, irradiation temperature, and material composition. For example, a rapid increase, followed by saturation, followed by slow coarsening and a decrease in number density of precipitates was predicted by models and confirmed experimentally for 0.3% Cu RPV steels irradiated at low neutron flux and 290°C [13]. As another example, it has been shown that an increase in the nickel content in irradiated RPV material correlates to an increase in both average radius and number density of copper-rich precipitates [16]. Further, changes in the irradiation temperature particularly in the range of about 250-300°C, as well as the neutron flux has been shown to strongly affect how the microstructure evolves over increasing neutron fluence [13, 17, 18]. The following sections provide a discussion on other possible contributions of microstructural features to β, in terms of reported microstructural evolutions over the relevant irradiation conditions in the current study.

Effects of Neutron Flux and Composition

The effect of higher fluxes typical of test reactors depends on the combination of copper content, irradiation temperature, and neutron fluence [13, 19]. It has been shown that in low Cu steels, higher flux typical of test reactors can produce increased hardening at higher fluence due to an increased amount of unstable matrix defects (UMDs) [13]. In contrast, in higher Cu steels, these UMDs act as sinks to delay precipitation from radiation-enhanced diffusion [13], and thus delay or reduce hardening. This flux-dependent regime has been estimated to begin at fluxes above about $5x10^{11}$ n/(cm^2-s) at T_{ir} = 290°C [18]. So, it is likely that these flux-related effects occur and cause different effects in the trend of $\Delta\beta$ in the lower temperature samples of irradiated JRQ and JFL at T_{ir} = 255°C.

Recall that the JFL samples contained 0.01% Cu (low-copper steel), and the JRQ samples contained 0.14% Cu (medium-copper steel). It has been shown that the dominating hardening mechanism in low-copper steels are other defects such as point defect clusters and manganese-nickel precipitates [13, 19]. It is plausible that these defects, as well as UMDs as suggested in [13], have formed in the high fluence samples of the low-Cu JFL material, creating more pinning points for dislocations and thus causing a decrease in β, which would align with the experimental results.

Effects of Irradiation Temperature

Irradiation hardening due to matrix features (namely vacancy-solute cluster complexes) has been shown to increase with decreasing irradiation temperature, since matrix features are more thermally stable at lower temperatures [13, 17]. A lower irradiation temperature has also been shown to increase both the volume fraction and number density of precipitates, while decreasing the radius of the precipitates in the range of T_{ir} = 270-310°C [16]. This indicates that it is expected that there should be a smaller number density of precipitates in the JRQ at 290°C compared to JRQ at 255°C at the common neutron fluence of $5x10^{19}$ n/cm^2. Therefore, it can be assumed that the critical number density of precipitates, N_{cr}, has not yet been reached in the JRQ T_{ir} = 290°C samples and thus β is expected to increase generally with increasing N, since $N<N_{cr}$ in this case. This can potentially explain the differences in $\Delta\beta$ in JRQ at roughly $5x10^{19}$ n/cm^2

for T_{ir} = 290°C ($\Delta\beta$ = +18%) and T_{ir} = 255°C ($\Delta\beta$ = +97%). Small angle neutron scattering (SANS) measurements could confirm this.

Post-irradiation Annealing

Post-irradiation annealing (PIA) has been shown to recover some of the irradiation-induced embrittlement in RPV steels [13, 20-22]. Nanstad et al. [21] conducted Charpy impact testing on the JRQ samples investigated in the current work, and showed almost full recovery of the irradiation-induced ductile-brittle transition temperature shift from the annealing treatment. In a follow-up study, atom probe tomography (APT) experiments showed a decrease in number density of copper-rich precipitates of about an order of magnitude [22]. The remaining precipitates in the microstructure were significantly larger, and were only observed near grain boundaries. Follow-up characterizations are needed to fully quantify the changes in number density and size of precipitates in the PIA state, but the APT results showed that annealing caused most of the copper to dissolve in the matrix, while the remaining copper precipitates grew and coarsened. This effect of PIA has been shown in other studies, for example with VVER-440 weld material interrogated with APT and positron annihilation spectroscopy (PAS) [23, 24], and with SANS measurements of high-copper RPV weld materials [24].

To isolate contributions to β from annealing effects on the irradiated microstructure, an unirradiated JRQ sample was annealed with the same schedule as the post-irradiation annealing (460°C/18h). A slight increase in β of 7% was measured in the unirradiated and annealed sample, compared to the purely unirradiated sample. These results are shown in Figure 4, in comparison with the change in β due to annealing in the irradiated samples, where a clear decrease of 23-26% was seen from irradiated to annealed state. Since no (or at least very few) precipitates are expected to be present in the unirradiated sample, the results clearly show that the change in β from PIA is due to changes specific to the irradiated microstructure.

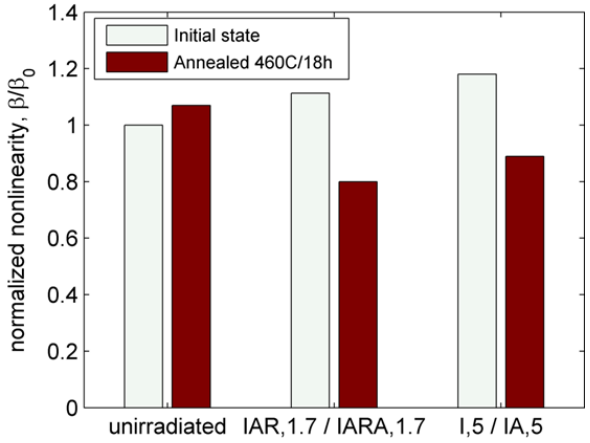

Figure 4: Dependence of β on annealing microstructural for unirraidated JRQ and irradiated JRQ (T_{ir} = 290°C).

The number density of precipitates in I,5 and IAR,1.7 samples should be below N_{cr}. Therefore, as precipitates are removed from the microstructure, N should still be below N_{cr}, and as such β should generally decrease as indicated by Equation (4) and Figure 6. Experimental evidence clearly shows this decrease in β. It is also possible that the coarsened precipitates remaining in the annealed microstructure have become incoherent with the matrix. The stress surrounding incoherent precipitates is significantly less than coherent precipitates, such that the precipitate-pinned dislocation model no longer applies.

Re-irradiation Effects

It has been shown that microstructural evolution during re-irradiation following PIA follows a different path than a purely irradiated microstructure [22, 23]. Nanstad et al. [22] conducted atom probe tomography investigations on the current samples, and they reported that re-irradiation does cause copper-rich precipitates to form with a number density similar to that in

the irradiated only condition, but with a smaller radius. If only considering the precipitate-pinned dislocation contribution to the nonlinearity parameter, the measured β should scale by $(r_{IAR}/r_I)^3$ when comparing a purely irradiated sample to an irradiated-annealed-re-irradiated sample to the same total fluence. Here, r_{IAR} is the radius of precipitates in the IAR condition, and r_I is the radius of precipitates in the irradiated condition.

Note that the samples at the lower neutron fluence levels for JRQ at T_{ir} = 290°C were given an annealing treatment when 50% of the target fluence was reached. This annealing was shown to recover a significant portion of the change in ductile- brittle transition temperature due to irradiation [21, 22]. So it is possible that a more representative measure of neutron fluence in terms of microstructural features is only the amount of neutron fluence received during the re-irradiation. In other words, 0.25×10^{19} n/cm^2 (instead of 0.5×10^{19} n/cm^2) might be a more representative fluence for sample IAR,0.5, and 0.85×10^{19} n/cm^2 (instead of 1.7×10^{19} n/cm^2) might be a more representative fluence for sample IAR,1.7. However, re-irradiation following post-irradiation annealing has been shown in some cases to follow a different path for microstructural evolution compared to changes due to the initial irradiation [23]. For example, Kuramoto and co-authors [23] investigated re-irradiation effects in VVER-440 type weld material, and concluded from APT and PAS studies that matrix defects are the primary hardening mechanism in the re-irradiated state. So, it is possible that matrix defects contribute to the measured β in IAR samples measured in the current study. It has been shown that defects such as vacancies can act in the same way as precipitates in terms of pinning points to dislocations [25]. It is also possible that these matrix defects respond as a different mechanism for contributing to the nonlinearity parameter. Further studies are needed to fully realize the effects on β from microstructural evolution during re-irradiation.

5. NLU to Quantify Remaining Life

Consider research that investigates second harmonic generation in Rayleigh surface waves propagating in 9%Cr ferritic martensitic steel. Previous experimental results show that nonlinear ultrasound is sensitive to certain microstructural changes in materials such as those due to thermal embrittlement and precipitation hardening. This research measures the ultrasonic nonlinearity parameter as an indicator of thermal damage in 9%Cr ferritic martensitic steel specimens. The specimens are isothermally aged for different holding periods to induce progressive changes in the microstructure and to obtain different levels of thermal damage. As thermal aging progresses, the existing dislocations are annihilated in the beginning and precipitates are formed; these microstructural evolutions lead to large changes in the measured nonlinearity parameter, β. Nonlinear ultrasonic experiments are conducted for each specimen using a wedge transducer for generation and an air-coupled transducer for detection of Rayleigh surface waves. The amplitudes of the first and second order harmonics are measured as a function of propagation distance, and these amplitudes are used to obtain the relative nonlinearity parameter at different aging stages. A possible scenario for the microstructural evolution during thermal aging is proposed based on the results from the nonlinear ultrasonic measurements, scanning electron microscopy (SEM), and Rockwell HRC hardness. These results indicate a clear trend that the measured nonlinearity parameter is sensitive to variations in dislocation and precipitate density, and thus can be useful in tracking microstructural changes in this material during thermal aging.

Figure 5(a) summarizes nonlinear ultrasonic measurements conducted in this research. The normalized nonlinearity parameter β is plotted with respect to the aging time in hours. The measured values of the nonlinearity parameter β are normalized by the mean value of the untreated specimen. The error bars indicate the maximum variation of the results for each specimen. The maximum error was 10% for the last specimen, which still looks acceptable since the trend is clearly recognizable. Figure 5(a) shows an initially rapid decrease of β, followed by an increase after the aging time of 500 h. In the first 500 h, the nonlinearity parameter drops from 100% to about 70%. This drop of 30% can be explained by the reduction of the dislocation density. The further increase until 3000 h is reasonable because the precipitated particles start to form and grow. At 3000 h, the nonlinearity parameter β reaches a value of 113%. Due to these significant measured changes of β, the conclusion can be drawn that the nonlinearity parameter is very sensitive to the microstructural evolution including dislocations and precipitations in this material.

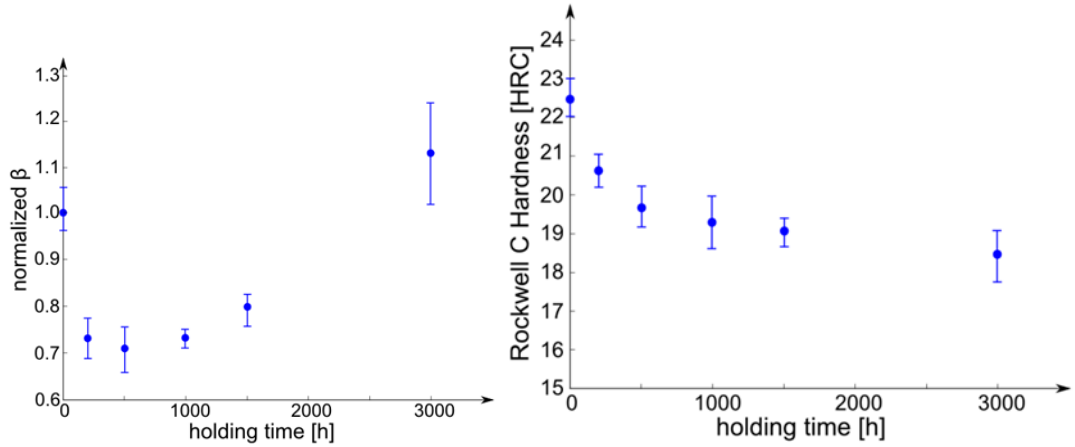

Fig. 5: Nonlinearity parameter β (a) normalized by the mean value of specimen 1 and Rockwell C hardness (b) over holding time.

This trend is supported by Park et al. [26] who also measure the nonlinearity parameter for a 10.5%Cr steel with a different composition of alloying elements. This study investigates a similar material for several aging temperatures and their results of the nonlinearity parameter show a trend similar to that shown in Figure 5(a). Rockwell Hardness Test and Metallurgical Analysis

A clear decrease of hardness with increasing holding time is observed in Figure 5(b) for the heat treated specimens. The modified 9%Cr steel indicates an initially drastic decrease up to a holding time of 500 h. The averaged value drops from 22.5 HRC to 19.8 HRC within 500 h. After that time, the hardness gradually reduces to a value of 18.5 HRC. A similar trend of rapid decrease, followed by a slight decrease in hardness is reported by Jones et al. [27] who investigated the behavior for different temperatures and found out that with an increasing temperature, the initial slope becomes steeper. The trend reveals that the hardness is not the best indicator for thermal damage because there is no significant measurable change after 500 h. Scanning electron microscopy (SEM) is performed with a JOEL JSM-7600F microscope. Furthermore, element mapping and energy dispersive X-ray microanalyses (EDX) are conducted to emphasize the distribution and concentration of the three most important alloying elements: chromium, molybdenum and iron. To obtain the metallographic results, the specimens are

carefully ground with emery paper to a grade of 1200 and subsequently polished with a 1 μm diamond solution and cloth. The microstructure is revealed using a Villela's reagent, which is a common metallographic etchant for heat treated steels and martensitic stainless steels. It contains 100 m*l* ethanol, 5 m*l* HCl and 1 g of picric acid. Initially, particles are seen to be evenly distributed in the matrix and at the boundaries of grains. Both inter and intra granular precipitates of different morphologies are observed in the image, while most of them are aligned along the grain boundaries. While Figure 6(a) shows very fine intra lath precipitates prior to the heat treatment with particle radii $r_p << 1$ μm, Figure 6(c) shows the effect of the aging treatment as a carbide growing mechanism. It is noticed that the precipitation is uniform and the density of precipitates is higher; furthermore, the micrographs show larger precipitates. As observed in Figures 6(b), iron (green) and molybdenum (blue) are homogeneously distributed, whereas a higher concentration of chromium (purple) shows up in some areas.

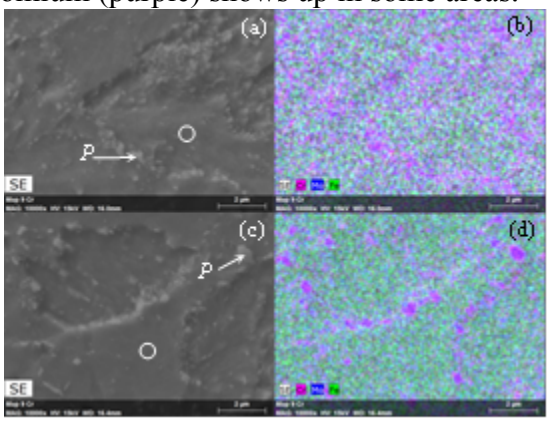

Fig.6: Element mapping of specimen with holding time of 0 h (left) and 3000 h (right).

However, it still has some level of regularity in its distribution. As aging time progresses, the diffusion of chromium is evident concentrating in the bigger particles as depicted in Figure 6(d). Table 2 summarizes the results of the EDX at the particles and matrix indicated in Figures 6(a) and 7(c), where the element concentrations in the matrix (circle) and a particle (*P*) are determined before and after 3000 h heat treatment.

Table 2. Element concentrations

	Base material		3000 h	
Element	matrix [wt. %]	particle [wt. %]	matrix [wt. %]	particle [wt. %]
Fe	85.04	75.23	88.59	36.68
Cr	7.02	11.17	7.12	47.27
Mo	0.43	0.99	0.4	4.53
C	4.52	9.48	3.29	8.64

The chromium concentration after 3000 h holding time is four times higher than that in the untreated specimen. When the precipitated particle in the base material is compared with that after aging, the chromium content increases from 11.17% to 47.27%, leading to a sharp decline of the iron concentration from 75.23% to 36.78%. From Table 3, it can be seen that the carbon (8.8%), chromium (11.17%) and molybdenum (0.99%) are richer in the precipitated particles than in the matrix. The results lead to the assumption that the particles may be a chromium

carbide type. Furthermore, the particle size increases for each further aged specimen and after 3000 h; some particles reach a size of about 0.8 μm in diameter. In general, the precipitation sequence depends mainly on the composition of the steel, but the diffusivities of the alloy elements and the ease of nucleation are also important parameters determining the favored carbide phases [27].

Figure 7 shows the qualitative trends of the dislocation density (dashed line) and the radius of precipitated particles (dotted line) that are extracted from other studies on similar steels ([26, 28] and [29-31] respectively), as well as the experimentally measured acoustic nonlinearity and hardness. The entire behavior is divided into two phases: an initial phase which is dominated by decreasing contributions to β; followed by a second phase which is dominated by increasing contributions on β. The initial phase clearly shows a simultaneous decrease in the hardness and nonlinearity parameter. The decrease in nonlinearity up to 500 h is mainly caused by the reduction of dislocation density $\Lambda^{(d)}$ and the precipitate nucleation process. The characteristics of the experimentally measured β and hardness allows the conclusion to be drawn that the microstructural changes associated with the decreasing dislocation density is the dominate mechanism. This phase where the value of β decreases is followed by a phase where the growth of precipitated particles dominates, causing an increase in the nonlinearity parameter, β. The nonlinearity at the aging time of 3000 h exceeds even the starting value by approximately 13%. In this increasing phase, the dislocation density changes very slowly, and simultaneously the earlier nucleated particles grow in size. The results obtained in these measurements imply that the behavior after 500 h is probably dominated by the contribution of the growing precipitates. However, this hypothesis needs to be further investigated since the quantitative effects of dislocations and precipitated particles on β are yet to be determined. Thus, a more precise investigation into the microstructural evolution is necessary through the determination of the dislocation density $\Lambda^{(d)}$, the exact size of the particles r_p and their volume fraction f_p. Nonetheless, there is a significant change in β over aging time in Figure 7, which allows an assessment of the stage of thermal aging. Note that the specimens show no signs of any other damage or cracks until 3000 h.

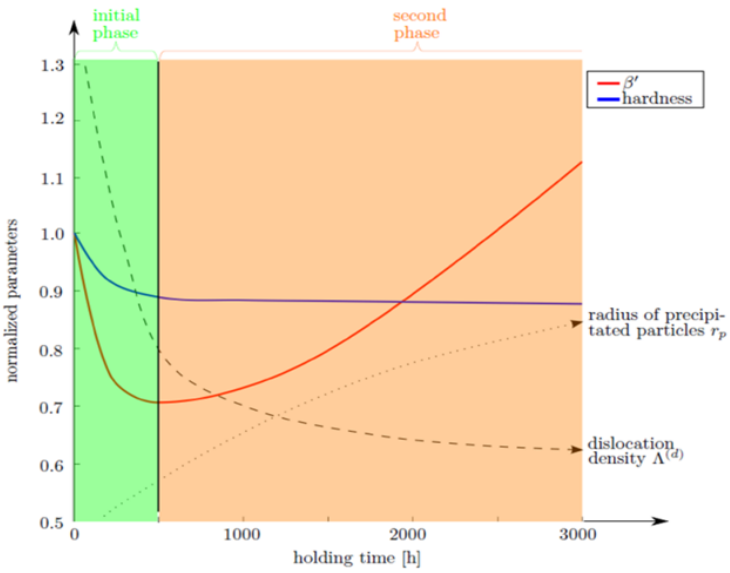

Fig. 7: Comparison of hardness and ultrasonic results with the qualitative trend of the dislocation density and radius of precipitated particles.

Overall, this portion of the research demonstrates that, compared with linear ultrasonic attenuation and velocity, the acoustic nonlinearity parameter β is more sensitive to changes in the microstructure and β is a useful parameter to predict the stage of thermal damage in 9%Cr ferritic martensitic steel. The nonlinear ultrasonic results indicate an initially rapid decrease, followed by

an increase in the nonlinearity parameter β. The initial phase of decreasing material nonlinearity is dominated by the decrease of dislocation density. In the second phase, the reduction of the dislocation density slows down and the precipitated particles form and grow, which leads to the measured increase in the acoustic nonlinearity parameter. The scanning electron microscopy and hardness measurements support the results obtained from the nonlinear ultrasonic measurements. The monotonic decrease in hardness serves as an indicator for the decrease of the dislocation density, since the curve of the hardness can be described by the dissolution of lath martensite that contains a high dislocation density. Furthermore, the scanning electron microscopy reveals the growth of the precipitated particles as the aging process progresses. The untreated specimen contains small, evenly distributed chromium containing precipitates. SEM images show that the further the aging process advances, the bigger the precipitates are. The nonlinearity parameter β provides an understanding of, and information on, the microstructure and hardness. However, due to the nature of the complex phase transformations that occurs during aging, for an absolute assessment of the microstructure state with the nonlinearity parameter β, one needs to develop a quantitative model that describes this evolution process and the corresponding changes in β.

References

[1] K.H. Matlack, J.-Y. Kim, J.J. Wall, J. Qu, L.J. Jacobs, M.A. Sokolov, J. Nucl. Mater. 448 (2014) 26-32.
[2] K.H. Matlack, J.J. Wall, J.-Y. Kim, J. Qu, L.J. Jacobs, H.-W. Viehrig, Evaluation of radiation damage using nonlinear ultrasound, J. Appl. Phys., 111 (2012) 054911-054913.
[3] A. Hikata, B.B. Chick, C. Elbaum, Dislocation contribution to the second harmonic generation of ultrasonic waves, J. Appl. Phys., 36 (1965) 229-236.
[4] J.H. Cantrell, X.G. Zhang, Nonlinear acoustic response from precipitate-matrix misfit in a dislocation network, J. Appl. Phys., 84 (1998) 5469-5472.
[5] J. Frouin, S. Sathish, T.E. Matikas, J.K. Na, Ultrasonic linear and nonlinear behavior of fatigued Ti-6Al-4V, J. Mater. Res., 14 (1998) 1295-1298.
[6] J.-Y. Kim, L.J. Jacobs, J. Qu, J.W. Littles, Experimental characterization of fatigue damage in a nickel-base superalloy using nonlinear ultrasonic waves, J. Acoust. Soc. Am., 120 (2006) 1266-1273.
[7] S.V. Walker, J.-Y. Kim, J. Qu, L.J. Jacobs, Fatigue damage evaluation in A36 steel using nonlinear Rayleigh surface waves, NDT&E Int., 48 (2012) 10-15.
[8] A. Viswanath, B.P.C. Rao, S. Mahadevan, P. Parameswaran, T. Jayakumar, B. Raj, Nondestructive assessment of tensile properties of cold worked AISI type 304 stainless steel using nonlinear ultrasonic technique, J. Mater. Process. Technol., 211 (2011) 538-544.
[9] D.C. Hurley, D. Balzar, P.T. Purtscher, Nonlinear ultrasonic assessment of precipitation hardening in ASTM A710 steel, J. Mater. Res., 15 (2000) 2036-2042.
[10] J.W. Martin, The Metallography of Deformed Alloys, and Theories of the Mechanisms of Hardening, in: Precipitation Hardening, Pergamon Press, Great Britian, 1968, pp. 60-63.
[11] J.H. Cantrell, W.T. Yost, Determination of precipitate nucleation and growth rates from ultrasonic harmonic generation, Appl. Phys. Lett., 77 (2000) 1952-1954.
[12] G.R. Odette, G.E. Lucas, Embrittlement of nuclear reactor pressure vessels, JOM, 53 (2001) 18-22.

[13] G.R. Odette, G.E. Lucas, Recent progress in understanding reactor pressure vessel steel embrittlement, Radiation Effects and Defects in Solids: Incorporating Plasma Science and Plasma Technology, 144 (1998) 189-231.
[14] E. Meslin, M. Lambrecht, M. Hernandez-Mayoral, F. Bergner, L. Malerba, P. Pareige, B. Radiguet, A. Barbu, D. Gomez-Briceno, A. Ulbricht, A. Almazouzi, Characterization of neutron-irradiated ferritic model alloys and a RPV steel from combined APT, SANS, TEM, and PAS analyses, J. Nucl. Mater., 406 (2010) 73-83.
[15] A. Ulbricht, J. Bohmert, H.-W. Viehrig, Microstructural and mechanical characterization of radiation effects in model reactor pressure vessel steels, J. ASTM Int., 2 (2005) 151-164.
[16] E.D. Eason, G.R. Odette, R.K. Nanstad, T. Yamamoto, A physically based correlation of irradiation-induced transition temperature shifts for RPV steels, ORNL/TM-2006/530, 2006.
[17] E.D. Eason, G.R. Odette, R.K. Nanstad, T. Yamamoto, A physically-based correlation of irradiation-induced transition temperature shifts for RPV steels, J. Nucl. Mater., 433 (2013) 240-254.
[18] G.R. Odette, T. Yamamoto, D. Klingensmith, On the effect of dose rate on irradiation hardening of RPV steels, Philosophical Magazine, 85 (2005) 779-797.
[19] R.E. Stoller, The effect of neutron flux on radiation-induced embrittlement in reactor pressure vessel steels, in: M.L. Grossbeck, T.R. Allen, R.G. Lott, A.S. Kumar (Eds.) Effects of Radiation on Materials: 21st International Symposium, ASTM STP 1447, ASTM International, West Conshohocken, PA, 2004, pp. 326-337.
[20] E.D. Eason, J.E. Wright, E.E. Nelson, G.R. Odette, E.V. Mader, Embrittlement recovery due to annealing of reactor pressure vessel steels, Nucl. Eng. Des., 179 (1998) 257-265.
[21] R.K. Nanstad, P. Tipping, R.D. Kalkhof, M.A. Sokolov, Irradiation and Post-Annealing Reirradiation Effects on Fracture Toughness of RPV Steel Heat JRQ, in: M.L. Grossbeck, T.R. Allen, R.G. Lott, A.S. Kumar (Eds.) The Effects of Radiation on Materials: 21st International Symposium, ASTM STP 1447, ASTM International, West Conshokocken, PA, 2004, pp. 149-163.
[22] R.K. Nanstad, M. Niffenegger, R.D. Kalkhof, M.K. Miller, M.A. Sokolov, P. Tipping, Fracture Toughness, Thermo-Electric Power, and Atom Probe Investigations of JRQ Steel in I, IA, IAR, and IARA Conditions, J. ASTM Int., 2 (2005) 1-17.
[23] A. Kuramoto, T. Toyama, Y. Nagai, K. Inoue, Y. Nozawa, M. Hasegawa, M. Valo, Microstructural changes in a Russian-type reactor weld material after neutron irradiation, post-irradiation annealing and re-irradiation studied by atom probe tomography and positron annihilation spectroscopy, Acta Materialia, 61 (2013) 5236-5246.
[24] G.R. Odette, B.D. Wirth, J. Nucl. Mater. 251 (1997) 157-171.
[25] J.H. Cantrell, Quantitative assessment of fatigue damage accumulation in wavy slip metals from acoustic harmonic generation, Philosophical Magazine, 86 (2006) 1539-1554.
[26] J. Park, M. Kim, B. Chi,and C. Jang. Correlation of metallurgical analysis and higher harmonic ultrasound response for long term isothermally aged and crept FM steel for USC TPP turbine rotors. NDT&E International, Vol. 54: 159-165, 2013.
[27] W. B. Jones, C. R. Hills, D. H. Polonis. Microstructural evolution of modified 9Cr-1Mo steel. Metallurgical Transactions A, Vol.22: 1049-1058, 1991.
[28] K. Sawada, K. Miyahara, H. Kushima, K. Kimura. Contribution of microstructural factors to hardness change during creep exposure in mod. 9Cr-1Mo steel. ISIJ International, Vol. 45, 2005.

[29] H. K. Danielsen and J. Hald. Influence of Z-phase on long-term creep stability of martensite 9 to 12%Cr steel. VGB Power Tech, Vol.5: 68-73, 2009.
[30] L. Cipolla, A. Gianfrancesco, D. Venditti, G. Cumino and S. Caminada. Microstructural evolution during long term creep tests of 9% Cr steel grades. Eighth International Conference on Creep and Fatigue at Elevated Temperatures, 2007.
[31] J. Hald. Microstructure and long-term creep properties of 9–12% Cr steels. International Journal of Pressure Vessels and Piping, Vol.85: 30-37, 2008.

U.S. DEPARTMENT OF ENERGY
Nuclear Energy

Nonlinear Ultrasonic Techniques to Monitor Radiation Damage in RPV and Internal Components

OVERVIEW

Purpose: Radiation damage reduces the fracture toughness of RPV steels and internals, and can leave them susceptible to irradiation assisted stress corrosion cracking (IASCC), which may in turn limit the lifetimes of some operating reactors. The ability to characterize radiation damage in the RPV and internals will allow a clearer definition of reactor safety margins and enable nuclear operators to set operation time thresholds for vessels and prescribe and schedule replacement activities for core internals.

Objectives:

- Demonstrate that nonlinear ultrasonics (NLU) is sensitive to radiation damage.
- Develop a physics-based materials model to track radiation damage
- Integrate sensing, modeling and uncertainty for remaining life estimation
- Use NLU to directly and quantitatively measure the remaining life in radiation damaged RPV and internal components.

IMPACT

Logical Path: The proposed effort is divided into three integrated tasks as shown in the Schematic in the third quadrant. Task 1: material sensing and monitoring with nonlinear ultrasound; Task 2: Physics-based material modeling for prediction and validation; and Task 3: Remaining life estimation by integrating sensing, modeling and uncertainty analysis.

Outcomes: Our vision is to develop a technique that enables operators to assess damage by making a limited number of NLU measurements in strategically selected critical reactor components during regularly scheduled outages. These measured data can then be used to determine the condition of these key components, from which remaining useful life can be predicted.

DETAILS

Principal Investigator: Laurence Jacobs, Georgia Tech, laurence.jacobs@coe.gatech.edu, 404-894-2344

Institution: Georgia Institute of Technology

Collaborators: Northwestern University, EPRI, PNNL

Duration: August 2012-August 2015 **Total Funding Level**: $877,000.

TPOC: Jeremy Busby

Federal Manager: Richard Reister

Workscope: LWRS-3

PICSNE Workpackage #: NU-12-GA-GT-0304-02 (Project 12-3306)

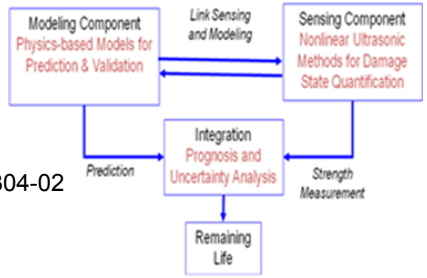

RESULTS

Overall, the research resulted in eight published papers, two currently under review and three in preparation. Radiation damage in RPV steels causes microstructural changes that leave the material in an embrittled state. Nonlinear ultrasound is sensitive to microstructural changes in metallic materials such as dislocations and precipitates.This research first demonstrated the sensitivity of the acoustic nonlinearity parameter to increasing neutron fluence in representative RPV steels. It then examined similar RPV steel samples that had a combination of irradiation, annealing, re-irradiation, and/or re-annealing to a total neutron fluence of 0.5-5x1019 n/cm2 (E > 1 MeV). As shown in the figure, the acoustic nonlinearity parameter generally increased with increasing neutron fluence, and consistently decreased from the Irradiated to the annealed state over different levels of neutron fluence. Since the main Contributor of irradiation damage is copper-Rich precipitates, 17-4PH stainless steel is thermally aged to study the effects of copper precipitates on the acoustic nonlinearity parameter. Results showed a decrease in the acoustic nonlinearity parameter with aging consistent with evidence of copper precipitation from TEM and APT.